Table VII shows the values of both these sets of torsion angles, along with those derived from the pseudorotational model. As might have been anticipated, the agreement between set b and the other two sets is not as good as between sets a and c. The vicinal coupling constants derived from the torsion angles in sets a and c differ at most by 0.4 Hz. Hence the assumption of trigonal symmetry leads to acceptable results.

Conclusions

The present solid-state data provide support for the previously proposed[5] atypical conformational equilibrium $^2E \rightleftharpoons {}_4E$ for 8-Br-xyloA in Me_2SO solution. The conclusions regarding conformation are affected to only a minor degree for a relatively broad range of assumed τ_m values (34–42°). The modified Karplus relationship of Haasnoot et al.[36] is far superior to the standard Karplus relationship for conformational analyses of xylofuranosyl nucleosides in solution. Finally, the dependence of $J_{3'4'}$ on sugar ring conformation obtained by quantum chemical calculations[34] is similar to that given by application of the relationship of Haasnoot et al.[36]

Acknowledgments. All crystallographic computations were carried out with programs written by Ahmed et al.[39] Figures 1 and 4 were drawn with the ORTEP program of Johnson.[40] The program BMFIT(III) of Nyburg[41] was used to prepare Figure 3. We are indebted to Dr. L. Dudycz for the synthesis of 8-Br-xyloA. M.C. and I.E. thank the National Research Council of Canada for Research Associateships. Part of this investigation was supported by the Polish National Cancer Research Program (PR-6).

Registry No. 8-Br-xyloA, 15830-78-1.

Supplementary Material Available: Anisotropic temperature parameters of the nonhydrogen atoms, coordinates and isotropic temperature parameters of hydrogen atoms, comparison of observed and calculated endocyclic bond angles in the furanose rings, deviations from least-squares planes, and observed and calculated structure amplitudes (24 pages). Ordering information is given on any current masthead page.

(39) Ahmed, F. R.; Hall, S. R.; Pippy, M. E.; Huber, C. P. *J. Appl. Crystallogr.* **1973**, *6*, 309–346.
(40) Johnson, C. K. ORTEP Report ORNL-3794 (2nd revision); Oak Ridge National Laboratory: Oak Ridge, TN, 1970.
(41) Nyburg, S. C., private communication.

Isolation, Purification, and Characterization of High-Valent Complexes from a Manganese Porphyrin Based Catalytic Hydrocarbon Activation System. Crystal and Molecular Structure of μ-Oxo-bis[azido(tetraphenylporphinato)manganese(IV)]

Bruce C. Schardt, Frederick J. Hollander, and Craig L. Hill*

Contribution from the Department of Chemistry, University of California, Berkeley, California 94720. *Received June 12, 1981*

Abstract: High-valent complexes have been isolated from the reactions of (tetraphenylporphinato)manganese(III) derivatives, $XMn^{III}TPP$, with iodosylbenzene in hydrocarbon or halocarbon solvents. When $X = N_3^-$ or OCN^-, dimeric μ-oxo-manganese(IV) porphyrin complexes, $[XMn^{IV}TPP]_2O$, **4**, are isolated. The dimer $[N_3Mn^{IV}TPP]_2O$ has been characterized by X-ray crystallography. Intense broad absorption bands near 800 cm^{-1} in the infrared spectra of the complexes have been assigned to Mn–O–Mn bands based on ^{18}O substitution. Magnetic susceptibility measurements give $\mu_{eff} = 2.0\ \mu_B$ for $[N_3Mn^{IV}TPP]_2O$. The complexes are EPR silent. $[N_3Mn^{IV}TPP]_2O$ crystallizes as a chlorobenzene solvate in space group *Pbcn*. The unit cell has $a = 21.208$ (5) Å, $b = 16.826$ (4) Å, and $c = 22.620$ (3) Å and contains four molecules. The structure was solved by the heavy-atom method and converged with a final $R = 0.094$. The $[N_3Mn^{IV}TPP]_2O$ molecule possesses rigorous crystallographic C_2 symmetry with both Mn atoms, the bridging oxo oxygen atom, and the ligating nitrogen atoms of each N_3 ligand lying on the twofold axis. The two Mn atoms are displaced from the mean N_4 planes toward the bridging oxygen by 0.10 and 0.08 Å. The average Mn–N(porphyrin) bond distance is 2.014 (19) Å. Two antiferromagnetically coupled d^3 Mn(IV) atoms is the best description of the ground state for the dimeric complexes, **4**. On the basis of the similarity of the properties observed for both solid-state and solution samples of the complexes, their structures are probably the same in solution as in the solid state.

High-valent metalloporphyrin complexes have come under increased study in recent years because of their importance in natural systems. For example, some of the most remarkable reactions that take place in the biosphere are the hydrocarbon C–H bond activation processes catalyzed by cytochrome P-450.[1] This class of heme containing monooxygenases occurs in a variety of forms of life where they are responsible for the selective oxidation of various hydrocarbons or for the catabolism of drugs or hormones.[1] In these processes cytochrome P-450 is capable of cleaving aromatic C–H bonds and also of cleaving unactivated alkane C–H bonds regiospecifically and stereospecifically.[1] The desire to understand the mechanism(s) of cytochrome P-450-catalyzed hydrocarbon hydroxylation processes and the need for selective and effective synthetic oxygenation catalysts have recently motivated numerous investigators to examine a variety of model hydroxylation systems.[2-8] Since the initial discovery by Groves

(1) Recent review of cytochrome P-450: (a) Coon, M. J.; White, R. E. "Metal Ion Activation of Dioxygen"; Spiro, T. G., Ed.; Wiley: New York, 1980; Chapter 2. (b) Gunsalus, I. C.; Sligar, S. G. *Adv. Enzymol. Relat. Areas Mol. Biol.* **1978**, *47*, 1. (c) Groves, J. T. In "Advances in Inorganic Biochemistry"; Eichhorn, G. L., Marzilli, L. G., Eds.; Elsevier/North Holland: New York, 1979; Vol. 1, Chapter 4. (d) Chang, C. K.; Dolphin, D. In "Bioorganic Chemistry"; van Tamelen, E. E., Ed.; Academic Press: London, 1978; Vol. IV, p 37.

(2) Review of early work (up through 1973) on chemical model systems for oxygenase enzymes: Hamilton, G. A. In "Molecular Mechanisms of Oxygen Activation"; Hayaishi, O., Ed.; Academic Press: New York, 1974; Chapter 10.

0002-7863/82/1504-3964$01.25/0

and co-workers that synthetic iron porphyrins can catalyze various hydrocarbon oxygenation processes by using iodosylbenzene as the source of reduced oxygen,[4a] extensive efforts have been made to isolate, purify, and characterize highly reactive intermediate metalloporphyrin complexes from several model oxygenation systems involving peroxides or oxoiodine reagents and synthetic metalloporphyrins.[4-8] High-valent intermediate metalloporphyrins from the M(porphyrin)–oxoiodine(III) systems, M = iron,[5] chromium,[6] and manganese,[7,8] have been studied. Recently our group and that of J. Groves published communications in this journal describing the reactions of (tetraphenylporphinato)manganese(III) derivatives with an excess of iodosylbenzene in hydrocarbon or mixed chlorocarbon/hydrocarbon solvents.[7,8] In contrast to the iron porphyrin iodosylbenzene systems,[4a,5] the yields of hydroxylated alkane products with the manganese porphyrin–iodosylbenzene system are high, and good yields of halogenated products are produced. High-valent manganese porphyrin complexes have also been shown to be capable of oxidizing water to dioxygen or hydrogen peroxide in both thermal[9] and photochemical[10] processes. Unfortunately the high-valent manganese porphyrin complexes in these water-activating systems are very reactive, relatively intractable, and thus no better characterized than the high-valent manganese porphyrin complexes involved in the catalytic hydrocarbon oxygenation systems. The unusual chemistry and photochemistry associated with these complexes cannot be properly understood without a more comprehensive characterization of the structural and physical properties of these species.

The insufficient characterization of high-valent manganese porphyrin complexes provides the impetus for the research presented in this paper. We recently established conditions under which monomeric six-coordinate manganese(IV) porphyrin complexes could be manipulated, and we reported the preparation, purification, and characterization by X-ray crystallography of one exemplary complex, dimethoxy(tetraphenylporphinato)manganese(IV), $Mn^{IV}TPP(OCH_3)_2$.[11,12] This paper specifically addresses the isolation, purification, and characterization of two dimeric μ-oxo-manganese(IV) porphyrin complexes, $[XMn^{IV}TPP]_2O$, from the catalytic hydrocarbon activation system, $XMn^{III}TPP$–iodosylbenzene, X = Cl^-, Br^-, I^-, and N_3^-,[7,13] and the X-ray crystallographic structural analysis of one representative complex, μ-oxo-bis[azido(tetraphenylporphinato)manganese(IV)], **1**. This last complex was the subject of a short communication.[14]

Experimental Section

Physical Measurements. Visible spectra were recorded on a Cary Model 118 spectrometer. Infrared spectra were recorded on a Perkin-Elmer 283 spectrometer. Solution samples were recorded in dichloromethane by using 0.10-mm sodium chloride cells. Solid samples were recorded as KBr pellets at two concentrations, 3 or 6 wt % sample in KBr. Brief grinding in the preparation of the KBr pellets and short scan times of 10 min were used to avoid thermal decomposition. After the IR spectra were taken, the samples were extracted from the KBr pellets with dichloromethane and their electronic spectra taken to determine the extent of decomposition. Magnetic moments were measured on a Gouy balance consisting of a Spectro-magnetic Industries electromagnet and a Mettler analytical balance. $HgCo(NCS)_4$ was used as a calibrant. Solution magnetic moments were measured by the Evans method.[15] X-Band EPR spectra were recorded on a Varian Model E-109 spectrometer with the probe thermostated at one of several temperatures between 8 and 300 K. Elemental analyses were performed by the Micro-analytical laboratory operated by the Department of Chemistry, University of California, Berkeley.

Materials. Methanol was distilled from $Mg(OMe)_2$. Ethyl ether was distilled from sodium benzophenone ketyl. The solvents dichloromethane, carbon tetrachloride, chlorobenzene, hexane, and heptane were stirred with concentrated sulfuric acid, washed with water, washed with aqueous KOH, washed again with water, dried with $MgSO_4$, and fractionally distilled from P_2O_5. Oxygen-18 enriched water (54 atom % ^{18}O) was obtained from Alfa. Iodosylbenzene (iodosobenzene) was made by literature methods.[16] $(OAc)Mn^{III}TPP$ was made by the method of Adler et al.[17] $XMn^{III}TPP$, X = N_3^-, OCN^-, Cl^-, and Br^-, were made by ligand exchange with $(OAc)Mn^{III}TPP$ by the procedure used by Ogoshi on the corresponding Fe complexes.[18]

Syntheses. Because the high-valent manganese porphyrin complexes reported in this paper are decomposed easily to manganese(III) species, the relatively inert solvents chlorobenzene, benzene, dichloromethane, carbon tetrachloride, and alkanes were used. Likewise, low temperatures and an inert atmosphere were required for most manipulations.

$[N_3Mn^{IV}TPP]_2O$, 1. To a green solution of 500 mg (0.704 mmol) of $N_3Mn^{III}TPP$ in 25 mL of chlorobenzene was added 500 mg (2.27 mmol) of iodosylbenzene. The mixture was stirred for 5 min and then filtered through a fine frit into 250 mL of heptane at −78 °C. The resulting brown precipitate was collected, washed with heptane, and dried to give 450 mg of crude product (89% yield). Anal. I, <1.5.

A bulk sample of analytically pure **1** for physical and chemical studies was prepared by rapidly dissolving 500 mg of the crude precipitated material in 50 mL of carbon tetrachloride, filtering the solution, and then adding 25 mL of heptane to the supernatant dropwise. Black solvate-free microcrystals of **1** were immediately produced, and the more soluble green $XMn^{III}TPP$ decomposition products stayed in solution. The microcrystalline **1** was collected on a frit, washed sequentially with hexane, carbon tetrachloride, and hexane, and then dried in vacuo overnight to afford 390 mg (78% yield) of pure **1**.

Anal. Calcd for $C_{88}H_{56}Mn_2N_{14}O$: C, 73.64; H, 3.93; N, 13.66. Found: C, 73.45; H 4.13; N, 13.33; I, <0.1.

Crystals of $[N_3Mn^{IV}TPP]_2O$, 1, for X-ray Crystallography. Diffraction-quality single crystals of this complex could only be grown at room temperature (22 °C). $N_3Mn^{III}TPP$ (150 mg, 0.21 mmol) in 5 mL of chlorobenzene was stirred with 150 mg (0.68 mmol) of iodosylbenzene for 2 min. The resulting orange-brown solution of **1** was filtered to remove the insoluble, unreacted iodosylbenzene. The supernatant was partitioned into three $3 \times {}^1/_2$ in. test tubes and then layered with heptane. After 24 h, the resulting large crystals of a chlorobenzene solvate of **1** were collected by filtration, washed with hexane, and dried in vacuo.

$[OCNMn^{IV}TPP]_2O$. This complex was prepared by the same procedure used to prepare the $[N_3Mn^{IV}TPP]_2O$ dimeric complex. The complex was recrystallized to give 350 mg (69% yield) of purple microcrystals.

Anal. Calcd for $C_{90}H_{56}Mn_2N_{10}O_3$: C, 75.31; H, 3.93; N, 9.76. Found: C, 75.11; H, 4.33; N, 9.49; I, <0.1.

$[OCNMn^{IV}TPP]_2{}^{18}O$ (54 atom % ^{18}O). Method I. To a solution of 100 mg (0.141 mmol) $OCNMn^{III}TPP$ in 5 mL of chlorobenzene was added 0.40 mL (21.0 mmol) of $H_2{}^{18}O$ (54 atom % ^{18}O) and 100 mg (0.454 mmol) of iodosylbenzene. The mixture was stirred for 5 min and then filtered through a medium frit into 50 mL of heptane. The amorphous brown precipitate was collected, washed with heptane, and dried.

Method II. Flame-dried glassware and solvents freshly dried by distillation from P_2O_5 were required for this method. To a solution of 100 mg (0.151 mmol) $(OCN)Mn^{III}TPP$ in 5 mL of chlorobenzene was added 100 mg (0.454 mmol) of 54 atom % [^{18}O]iodosylbenzene. The mixture was stirred for 5 min and then filtered through a fine frit into 50 mL of

(3) Recent review addressing the mechanisms of metal-catalyzed oxygen insertion reactions: Groves, J. T. In "Metal-Ion Activation of Dioxygen"; Spiro, T. G., Ed.; Wiley: New York, 1980; Chapter 3.

(4) (a) Groves, J. T.; Nemo, T. E.; Myers, R. S. *J. Am. Chem. Soc.* **1979**, *101*, 1032–1033. (b) Mansuy, D.; Bartoli, J.-F.; Chottard, J.-C.; Lange, M. *Angew. Chem., Int. Ed. Engl.* **1980**, *19*, 909–910. (c) Gold, A.; Ivey, W.; Bowen, M. *J. Chem. Soc., Chem. Commun.* **1981**, 293–295.

(5) (a) Groves, J. T.; Kruper, W. J.; Nemo, T. E.; Myers, R. S. *J. Mol. Catal.* **1980**, *7*, 169–177. (b) Chang, C. K.; Kuo, M.-S. *J. Am. Chem. Soc.* **1979**, *101*, 3413–3415.

(6) Groves, J. T.; Kruper, W. J., Jr. *J. Am. Chem. Soc.* **1979**, *101*, 7613–7615.

(7) Hill, C. L.; Schardt, B. C. *J. Am. Chem. Soc.* **1980**, *102*, 6374–6375.

(8) (a) Groves, J. T.; Kruper, W. J., Jr.; Haushalter, R. C. *J. Am. Chem. Soc.* **1980**, *102*, 6375–6377. (b) Willner, I.; Otvos, J. W.; Calvin, M. *J. Chem. Soc., Chem. Commun.* **1980**, 964–965.

(9) (a) Porter, G. *Proc. R. Soc. London, Ser. A* **1978**, *362*, 281–303. (b) Tabushi, I.; Kojo, S. *Tetrahedron Lett.* **1975**, 305–308.

(10) Harriman, A.; Porter, G. *J. Chem. Soc., Faraday Trans. 2* **1979**, *75*, 1543–1552.

(11) Camenzind, M. J.; Hollander, F. J.; Hill, C. L., accepted for publication in *Inorg. Chem.*

(12) Abbreviation: TPP = *meso*-tetraphenylporphinato dianion ligand.

(13) A paper specifically addressing the mechanisms of these hydrocarbon oxidation processes will be published separately: Smegal, J. A.; Hill, C. L., manuscript in preparation.

(14) Schardt, B. C.; Hill, C. L. *J. Chem. Soc., Chem. Commun.* **1981**, 765.

(15) Evans, D. F. *J. Chem. Soc.* **1959**, 2003–2005.

(16) Lucas, H. J.; Kennedy, E. R.; Formo, M. W. "Organic Syntheses"; Wiley: New York, 1955; Coll. Vol. 3, pp 483–485.

(17) Adler, A. D.; Longo, F. R.; Kampas, F.; Kim, J. *J. Inorg. Nucl. Chem.* **1970**, *32*, 2443–2445.

(18) Ogoshi, H.; Watanabe, E.; Yoshida, Z.; Kincaid, J.; Nakamoto, K. *J. Am. Chem. Soc.* **1973**, *95*, 2845–2849.

Table I. Crystal and Data Collection Parameters for $[N_3Mn(tetraphenylporphyrin)]_2O \cdot 1.5C_6H_5Cl$

(A) Crystal Parameters at 25 °C[a,b]	
space group *Pbcn* (No. 60, D_{2h}^{14})	V = 8072 (4) Å^3
Z = 4	mol wt 1604.2 amu
a = 21.208 (5) Å	d_{calcd} = 1.320 g cm^{-3}
b = 16.826 (4) Å	d_{obsd} = 1.36 (2) g cm^{-3}
c = 22.620 (3) Å	μ_{calcd} = 4.06 cm^{-1}
(B) Data Measurement	
radiation	Mo Kα ($\bar{\lambda}$ = 0.710 73 Å)
monochrometer	highly oriented graphite ($2\theta_M$ = 12.2) perpendicular mode, assumed 50% perfect
reflections measd	$+h,+k,+l$
2θ range	3.0 → 45.0°
scan type	θ-2θ
scan speed (θ, deg/min)	1.34 (min), 5.0 (max)
scan width	$\Delta\theta$ = 0.70 + 0.347 tan θ
background	added 25% of scan width at each end of the scan
reflctns collected	5808
unique reflctns used in least squares	3276 with $F_o^2 > 3\sigma(F_o^2)$
std reflctns	10, 0, 2; 0, 12, 0; 0, 0, 12; measured every 2 h of X-ray exposure time (over the period of data collection no decay in intensity was observed)
orientation	checked after every 500 measurements (crystal orientation was redetermined if any of the three orientation check reflections was offset from its predicted position by more than 0.1°; reorientation was not performed during data collection)

[a] Unit cell parameters were derived by a least-squares fit to the setting angles of the unresolved Mo K$\bar{\alpha}$ components of 24 reflections with 2θ between 19° and 25°. [b] In this and all subsequent talbes the esd's of all parameters are given in parentheses, right-justified to the least-significant digit(s) given.

heptane. The brown precipitate was collected, washed with heptane, and dried. The electronic absorption spectra of $[OCNMn^{IV}TPP]_2{}^{18/16}O$ were identical with that of the natural abundance ^{16}O dimer and showed <1% $XMn^{III}TPP$ decomposition products.

X-ray Crystallography. Data Collection. Several well-shaped chlorobenzene solvate crystals of **1** prepared as described above were mounted on glass fibers in air. Preliminary precession photographs indicated orthorhombic Laue symmetry (*Pmmm*) and showed a rapid decrease in intensity with increasing (sin θ)/λ. The crystals were then mounted on an Enraf-Nonius CAD-4 automatic diffractometer and centered in the beam. After automatic searches of reciprocal space and indexing of the discovered reflections, the reflections were examined for intensity and peak width. The crystal used for data collection was the largest and had the sharpest peaks ($\Delta\omega$ = 0.20–0.35°). The peak width distribution was not uniform, peaks with high h being in general much wider than those with high k or l. Reflections with higher (sin θ)/λ were then located, and the cell dimensions were refined against their setting angles. The final cyrstal parameters are given in Table I, together with details of the data collection procedure. Checks of the intensities of equivalent reflections confirmed the choice of the orthorhombic cell, and inspection of intensities yielded systematic absences $0kl$, $k \neq 2n$, $h0l$, $l \neq 2n$, and $hk0$, consistent only with space group *Pbcn*.

Structure Solution and Refinement. The 5808 data collected were reduced to net intensities and then to structure factors and their estimated standard deviations by correction for scan speed and Lorentz and polarization effects.[19,21] Since analysis of several reflections located near

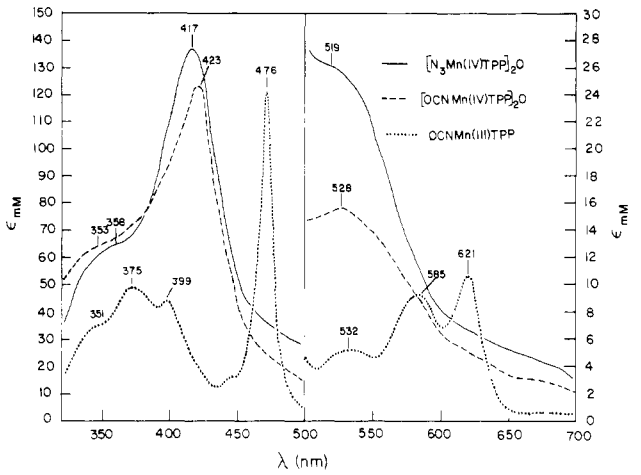

Figure 1. Electronic spectra of the high-valent Mn porphyrin complexes compared with the electronic spectra of a representative and typical Mn(III) porphyrin. $[N_3Mn^{IV}TPP]_2O$, (—); $[OCNMn^{IV}TPP]_2O$, (---); $OCNMn^{III}TPP$ (···). All spectra were recorded as ca. 1 mM chlorobenzene solutions. The spectra of $[N_3Mn^{IV}TPP]_2O$ and $OCNMn^{III}TPP$ were recorded at 22 °C and the spectra of $[OCNMn^{IV}TPP]_2O$ was recorded at 0 °C.

χ = 90°, which were measured at increments of 10° of rotation around the diffraction vector, showed a maximum variation in intensity of only ±2%, no absorption correction was performed. Rejection of systematic absences yielded 5249 unique reflections, of which 3276 had $F_o^2 > 3\sigma(F_o^2)$. The latter were used for the structure solution and refinement.

Attempts to solve the structure using MULTAN failed because almost all the reflections with large E values had $h + k = 2n$. This information, however, was consistent with the placement of two manganese atoms on the two-fold axis in space group *Pbcn* and allowed interpretation of the three-dimensional Patterson map to yield the two manganese positions and the coordinated nitrogen atom positions. The remaining nonhydrogen atoms were located via standard least-squares and Fourier techniques.

Refinement of all atoms with isotropic thermal parameters converged with R = 10.4%.[22] Inspection of the thermal parameters, bond distances, and bond angles in the chlorobenzene molecule of solvation showed grave discrepancies from expected values. A difference Fourier map was calculated with the contribution of the chlorobenzene removed, and an idealized (d_{Cl-C} = 1.67 Å, d_{C-C} = 1.40 Å, all angles = 120°) chlorobenzene molecule was force fit to the electron-density map. Inspection of the peak heights in the Fourier map revealed that both the chlorine and the carbon peaks were significantly lower than might be expected. Therefore, in addition to fixing the positional parameters of the six carbon atoms and the chlorine, constraints were applied to the occupancies and isotropic thermal parameters so that all occupancies and all carbon thermal parameters were forced to be equal. (The thermal parameter of the chlorine was allowed to refine independently.) Refinement then proceeded with all other atoms in the asymmetric unit given anisotropic thermal parameters. Convergence was reached with an occupancy factor for the chlorobenzene of 0.77 (1). The final residuals were R = 9.4%, wR = 13.4%, and GOF = 4.57 for 497 parameters refined against 3276 data.[22] The p factor used in the final cycles of refinement was 0.04. The final difference Fourier map showed a maximum peak of height 0.97 e$^-$/Å^3 located near the chlorine atom. The highest peak not located in the region of the chlorobenzene was of height 0.34 e$^-$/Å^3 and was located near C212.

Table II lists the positional and thermal parameters of all atoms in the asymmetric unit. A table of observed and calculated structure factors is available.

In least-squares refinement, the function minimized was $\sum w(|F_o| - |F_c|)^{-2}$. The scattering factors for the neutral atoms[23] were all corrected for the real and imaginary components of anomalous dispersion.[24]

(19) All calculations were performed on a PDP 11/60 by using locally modified Nonius-SDP[20] software.

(20) Structure Determination Package User's Guide, Apr 1980; Molecular Structure Corp.: College Station, TX 77840.

(21) The data reduction formulae are $F_o^2 = (\omega/Lp)(C - 2B)$, $\sigma_o(F_o^2) = (\omega/Lp)(C + 4B)^{1/2}$, $F_o = (F_o^2)^{1/2}$, and $\sigma_o(F) = \sigma_o(F_o^2)/2F_o$, where C is the total count in the scan, B the sum of the two background counts, ω the scan speed used in deg/min, and $(1/Lp) = \sin 2\theta(1 + \cos^2 2\theta_m)/(1 + \cos^2 2\theta_m - \sin^2 2\theta)$ the correction for Lorentz and polarization effects for a reflection with scattering angle 2θ and radiation monochromatized with a 50% perfect single-crystal monochrometer with scattering angle $2\theta_m$.

(22) $R = \sum||F_o| - |F_c||/\sum|F_o|$, $wR = [\sum w(|F_o| - |F_c|)^2/\sum wF_o^2]^{1/2}$, and GOF = $[\sum w(|F_o| - |F_c|)^2/(n_o - n_v)]^{1/2}$, where n_o is the number of observations, n_v is the number of variable parameters, and the weights w were given by $w = 4F_o^2/\sigma^2(F_o^2)$ and $\sigma^2(F_o^2) = [\sigma_o^2(F_o^2) + (pF^2)^2]$, where p is the factor used to lower the weight of intense reflections.

(23) Cromer, D. T.; Waber, J. T. "International Tables for X-ray Crystallography"; The Kynoch Press: Birmingham, England, 1974; Vol. IV, Table 2.2B.

Table II. Positional and Thermal Parameters and Their Estimated Standard Deviations[a]

atom	x	y	z	B(1,1)	B(2,2)	B(3,3)	B(1,2)	B(1,3)	B(2,3)
Mn1	0.0000 (0)	0.1674 (1)	0.2500 (0)	0.00142 (4)	0.00256 (8)	0.00167 (4)	0.0000 (0)	0.00008 (9)	0.0000 (0)
Mn2	0.0000 (0)	0.3776 (1)	0.2500 (0)	0.00111 (4)	0.00261 (7)	0.00161 (4)	0.0000 (0)	0.00011 (8)	0.0000 (0)
Cl	0.3320 (0)	0.2070 (0)	0.0820 (0)	12.6 (2)					
O(oxo)	0.0000 (0)	0.2710 (5)	0.2500 (0)	0.0020 (2)	0.0023 (3)	0.0016 (2)	0.0000 (0)	−0.0004 (4)	0.0000 (0)
N11	0.0618 (3)	0.1606 (5)	0.3172 (4)	0.0016 (2)	0.0028 (3)	0.0022 (2)	0.0005 (4)	−0.0004 (3)	0.0001 (5)
N12	0.0728 (3)	0.1624 (5)	0.1919 (3)	0.0012 (2)	0.0040 (4)	0.0015 (2)	0.0005 (4)	0.0002 (3)	−0.0000 (4)
N21	0.0200 (3)	0.3846 (4)	0.3375 (3)	0.0016 (2)	0.0024 (3)	0.0017 (2)	−0.0003 (4)	−0.0000 (3)	−0.0006 (4)
N22	0.0916 (3)	0.3802 (4)	0.2313 (3)	0.0008 (2)	0.0031 (3)	0.0015 (2)	−0.0003 (4)	0.0003 (3)	−0.0002 (4)
N1	0.0000 (0)	0.0486 (7)	0.2500 (0)	0.0029 (4)	0.0033 (5)	0.0031 (3)	0.0000 (0)	0.0000 (7)	0.0000 (0)
N2	0.0290 (9)	0.0096 (10)	0.2747 (8)	0.0043 (6)	0.0019 (6)	0.0026 (5)	−0.0001 (11)	−0.0009 (9)	0.0001 (9)
N3	0.0597 (13)	−0.0310 (13)	0.3040 (13)	0.0078 (10)	0.0033 (9)	0.0077 (9)	0.0012 (16)	−0.0070 (16)	0.0040 (16)
N4	0.0000 (0)	0.4961 (7)	0.2500 (0)	0.0028 (3)	0.0034 (5)	0.0025 (3)	0.0000 (0)	0.0002 (6)	0.0000 (0)
N5	−0.0140 (8)	0.5388 (11)	0.2935 (8)	0.0024 (5)	0.0044 (8)	0.0032 (5)	−0.0001 (11)	−0.0015 (9)	0.0000 (12)
N6	−0.0287 (12)	0.5815 (14)	0.3348 (11)	0.0059 (9)	0.0047 (10)	0.0045 (7)	−0.0000 (16)	0.0019 (14)	−0.0011 (16)
C11	0.0462 (4)	0.1544 (6)	0.3757 (4)	0.0020 (2)	0.0040 (5)	0.0013 (2)	0.0006 (6)	0.0004 (4)	0.0007 (5)
C12	0.1012 (5)	0.1329 (7)	0.4106 (5)	0.0016 (2)	0.0047 (5)	0.0024 (3)	0.0003 (6)	−0.0001 (4)	−0.0000 (7)
C13	0.1500 (5)	0.1262 (7)	0.3704 (5)	0.0026 (3)	0.0040 (5)	0.0020 (2)	−0.0001 (7)	−0.0011 (5)	0.0004 (6)
C14	0.1255 (5)	0.1454 (6)	0.3132 (4)	0.0020 (3)	0.0029 (4)	0.0020 (2)	0.0005 (6)	−0.0002 (4)	−0.0002 (6)
C15	0.1622 (4)	0.1495 (6)	0.2619 (4)	0.0017 (2)	0.0032 (4)	0.0016 (2)	0.0003 (5)	0.0003 (4)	0.0000 (5)
C16	0.1347 (5)	0.1620 (6)	0.2057 (4)	0.0020 (2)	0.0025 (4)	0.0022 (2)	0.0002 (6)	0.0004 (4)	0.0003 (5)
C17	0.1733 (5)	0.1718 (6)	0.1522 (4)	0.0023 (3)	0.0030 (4)	0.0018 (2)	0.0005 (6)	0.0003 (4)	0.0003 (6)
C18	0.1306 (5)	0.1754 (6)	0.1076 (5)	0.0026 (3)	0.0031 (5)	0.0023 (3)	−0.0001 (6)	0.0000 (5)	−0.0004 (6)
C19	0.0677 (4)	0.1686 (6)	0.1325 (4)	0.0015 (2)	0.0036 (4)	0.0015 (2)	−0.0003 (6)	0.0005 (4)	0.0001 (5)
C110	−0.0133 (5)	0.1628 (6)	0.4004 (4)	0.0020 (3)	0.0040 (4)	0.0018 (2)	0.0009 (6)	0.0003 (4)	0.0002 (6)
C111	0.2321 (4)	0.1397 (6)	0.2670 (4)	0.0016 (2)	0.0035 (4)	0.0020 (2)	0.0012 (6)	0.0003 (4)	0.0007 (5)
C112	0.2619 (5)	0.0790 (6)	0.2359 (5)	0.0018 (2)	0.0032 (4)	0.0025 (3)	0.0015 (6)	0.0009 (4)	0.0011 (6)
C113	0.3285 (5)	0.0678 (7)	0.2432 (5)	0.0027 (3)	0.0042 (5)	0.0026 (3)	0.0013 (7)	−0.0009 (5)	0.0012 (7)
C114	0.3616 (5)	0.1188 (7)	0.2818 (5)	0.0025 (3)	0.0048 (6)	0.0032 (3)	0.0023 (7)	0.0008 (6)	0.0009 (7)
C115	0.3307 (5)	0.1802 (7)	0.3121 (5)	0.0022 (3)	0.0059 (6)	0.0024 (3)	0.0007 (7)	−0.0002 (5)	0.0016 (7)
C116	0.2647 (5)	0.1900 (7)	0.3047 (4)	0.0016 (2)	0.0046 (5)	0.0021 (2)	0.0010 (6)	0.0002 (4)	0.0004 (6)
C117	−0.0171 (5)	0.1596 (7)	0.4670 (5)	0.0019 (3)	0.0061 (6)	0.0018 (2)	0.0013 (6)	−0.0003 (4)	0.0004 (7)
C118	0.0046 (6)	0.2269 (8)	0.4995 (6)	0.0031 (3)	0.0078 (7)	0.0026 (3)	0.0009 (10)	−0.0016 (6)	−0.0019 (8)
C119	0.0024 (6)	0.2212 (10)	0.5624 (6)	0.0035 (4)	0.0104 (9)	0.0024 (3)	0.0047 (10)	−0.0012 (6)	−0.0024 (9)
C120	−0.0176 (6)	0.1512 (11)	0.5894 (5)	0.0023 (3)	0.0132 (11)	0.0020 (3)	0.0022 (10)	−0.0001 (5)	0.0004 (10)
C121	−0.0375 (6)	0.0881 (10)	0.5577 (5)	0.0029 (3)	0.0101 (8)	0.0021 (3)	0.0034 (9)	0.0009 (6)	0.0031 (8)
C122	−0.0386 (5)	0.0901 (8)	0.4935 (5)	0.0023 (3)	0.0072 (7)	0.0025 (3)	0.0006 (8)	0.0009 (5)	0.0028 (8)
C21	−0.0226 (4)	0.4034 (6)	0.3816 (4)	0.0017 (2)	0.0028 (4)	0.0017 (2)	0.0004 (5)	0.0010 (4)	−0.0014 (5)
C22	0.0111 (4)	0.4236 (6)	0.4337 (5)	0.0017 (2)	0.0039 (4)	0.0022 (2)	−0.0005 (6)	−0.0003 (4)	−0.0021 (6)
C23	0.0741 (5)	0.4146 (7)	0.4226 (4)	0.0024 (3)	0.0038 (4)	0.0016 (2)	−0.0008 (6)	0.0007 (4)	−0.0015 (6)
C24	0.0789 (4)	0.3891 (6)	0.3619 (4)	0.0011 (2)	0.0032 (4)	0.0022 (2)	−0.0008 (5)	−0.0001 (4)	−0.0003 (6)
C25	0.1359 (4)	0.3746 (6)	0.3326 (4)	0.0014 (2)	0.0027 (4)	0.0016 (2)	−0.0004 (5)	0.0001 (4)	−0.0008 (5)
C26	0.1401 (4)	0.3676 (6)	0.2720 (4)	0.0015 (2)	0.0025 (4)	0.0021 (2)	−0.0003 (5)	0.0008 (4)	0.0005 (5)
C27	0.1985 (5)	0.3551 (5)	0.2384 (4)	0.0014 (2)	0.0026 (4)	0.0020 (2)	−0.0003 (5)	0.0009 (4)	0.0001 (5)
C28	0.1854 (4)	0.3663 (6)	0.1818 (4)	0.0017 (2)	0.0027 (4)	0.0018 (2)	−0.0005 (5)	0.0000 (4)	0.0008 (5)
C29	0.1182 (4)	0.3831 (6)	0.1774 (4)	0.0013 (2)	0.0026 (4)	0.0019 (2)	0.0003 (5)	−0.0000 (4)	0.0001 (5)
C210	−0.0879 (4)	0.4004 (6)	0.3752 (4)	0.0014 (2)	0.0033 (4)	0.0018 (2)	0.0000 (5)	0.0010 (4)	−0.0006 (5)
C211	0.1942 (4)	0.3674 (6)	0.3702 (4)	0.0010 (2)	0.0035 (4)	0.0020 (2)	0.0008 (5)	−0.0006 (4)	−0.0008 (6)
C212	0.1970 (5)	0.3164 (6)	0.4163 (4)	0.0018 (2)	0.0045 (5)	0.0014 (2)	0.0013 (6)	−0.0004 (4)	−0.0003 (6)
C213	0.2520 (6)	0.3064 (7)	0.4477 (5)	0.0030 (3)	0.0050 (6)	0.0023 (3)	0.0014 (8)	0.0004 (6)	−0.0010 (7)
C214	0.3077 (5)	0.3511 (7)	0.4315 (5)	0.0027 (3)	0.0054 (6)	0.0023 (3)	0.0008 (8)	−0.0005 (5)	−0.0002 (7)
C215	0.3049 (5)	0.4047 (7)	0.3873 (5)	0.0022 (3)	0.0051 (5)	0.0023 (3)	0.0004 (7)	−0.0002 (5)	−0.0011 (7)
C216	0.2474 (5)	0.4164 (7)	0.3547 (5)	0.0015 (2)	0.0039 (4)	0.0028 (3)	0.0002 (6)	−0.0009 (5)	−0.0017 (6)
C217	−0.1274 (4)	0.4178 (7)	0.4287 (4)	0.0016 (2)	0.0045 (5)	0.0019 (2)	−0.0015 (6)	0.0004 (4)	−0.0015 (6)
C218	−0.1672 (5)	0.4852 (7)	0.4282 (5)	0.0020 (3)	0.0050 (6)	0.0033 (3)	0.0008 (7)	0.0013 (5)	−0.0034 (7)
C219	−0.2039 (6)	0.5020 (9)	0.4764 (6)	0.0026 (3)	0.0085 (7)	0.0045 (4)	−0.0013 (9)	0.0031 (6)	−0.0058 (9)
C220	−0.2035 (6)	0.4543 (9)	0.5243 (6)	0.0033 (3)	0.0093 (7)	0.0037 (3)	−0.0056 (9)	0.0033 (6)	−0.0066 (8)
C221	−0.1631 (6)	0.3859 (9)	0.5271 (5)	0.0045 (4)	0.0093 (8)	0.0020 (3)	−0.0073 (9)	0.0014 (6)	−0.0026 (8)
C222	−0.1245 (6)	0.3667 (7)	0.4786 (5)	0.0032 (3)	0.0055 (6)	0.0025 (3)	−0.0034 (8)	0.0010 (5)	−0.0017 (7)

atom	x	y	z	B, Å²	atom	x	y	z	B, Å²
C1	0.3430 (0)	0.2970 (0)	0.1110 (0)	7.4 (5)	C4	0.3700 (0)	0.4440 (0)	0.1660 (0)	7.4 (0)
C2	0.3620 (0)	0.3000 (0)	0.1700 (0)	7.4 (0)	C5	0.3510 (0)	0.4410 (0)	0.1070 (0)	7.4 (0)
C3	0.3740 (0)	0.3720 (0)	0.1970 (0)	7.4 (0)	C6	0.3380 (0)	0.3680 (0)	0.0800 (0)	7.4 (0)

[a] The form of the anisotropic thermal parameter is $\exp[-(B(1,1)h^2 + B(2,2)k^2 + B(3,3)l^2 + B(1,2)hk + B(1,3)hl + B(2,3)kl)]$.

Results

Electronic Spectra. The electronic absorption spectra of both dimeric complexes $[XMn^{IV}TPP]_2O$, $X = N_3^-$ and OCN^-, and a representative manganese(III) porphyrin complex, $OCNMn^{III}TPP$, are presented in Figure 1.

The characteristic absorption bands in the spectra of the high-valent complexes are the broad Soret band at 417–423 nm, the broad absorption in the 502–530-nm region, and a broad shoulder at 353–358 nm.

The electronic spectra of the manganese(III) porphyrin complexes are quite different from those of the high-valent complexes. The intense Soret band in the region of 476 nm and absorption bands near 585 and 621 nm are characteristic of manganese(III) porphyrin complexes and are not present in the oxidized species. The extinction coefficients of the Soret bands per manganese atom of the high-valent complexes are about half those of the Mn(III) complexes. Due to the differences in both the absorption maxima

(24) Cromer, D. T. ref 23, Table 2.3.1.

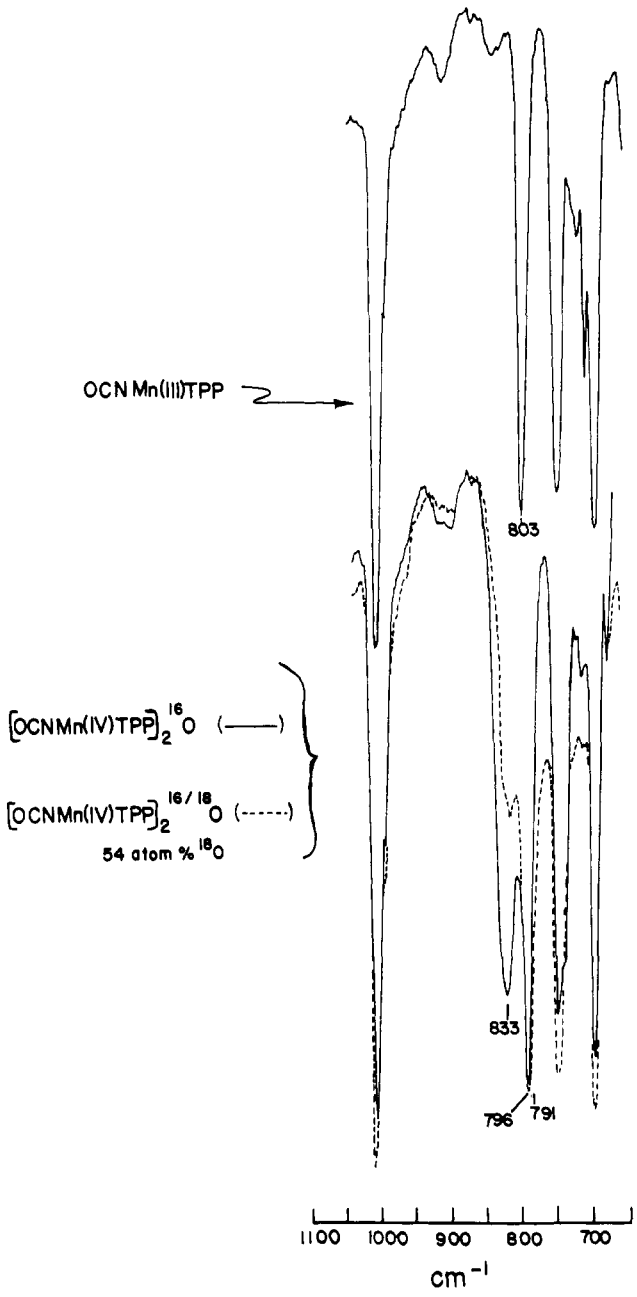

Figure 2. Comparison of the infrared spectra of OCNMnTPP, ^{16}O-labeled $[OCNMnTPP]_2O$, and 54 atom % ^{18}O-labeled $[OCNMnTPP]_2O$.

and extinction coefficients, the electronic spectra provide a rapid and quantitative assessment of the degree of decomposition of the high-valent species to Mn(III) complexes.

All the high-valent complexes decompose to Mn(III) with rates that are highly solvent and temperature dependent. At room temperature, 23 °C, in chlorobenzene, the half-life of the decomposition of the dimer complexes is ca. 24 h.

Infrared Spectra. Most of the absorption bands observed in the infrared spectra of the dimers and the manganese(III) porphyrins are due to the porphyrin ligand itself. These bands are only slightly affected by differences in the oxidation state and coordination geometry of the ligated metal.

An infrared spectral feature common to both of the high-valent complexes is an intense broad absorption band in the region of 800 cm^{-1}. This band is present in both the solution and solid-state spectra and absent from those of the $XMn^{III}TPP$ complexes. Figure 2 illustrates this for the complex $[(OCN)Mn(TPP)]_2O$. The position of this band in $[N_3Mn(TPP)]_2O$ is 794 cm^{-1}. Upon labeling of these complexes with ^{18}O using ca 50 atom % [^{18}O]iodosylbenzene, the intensity of this band decreases. The presence of strong porphyrin absorptions in this region of the spectrum prevents the observation of a new peak for the ^{18}O-labeled compounds. However, one observes increased intensity ca. 40–50 cm^{-1} lower in frequency. This is in qualitative agreement with theory ($\nu_{18} \simeq 0.95\nu_{16}$).[25]

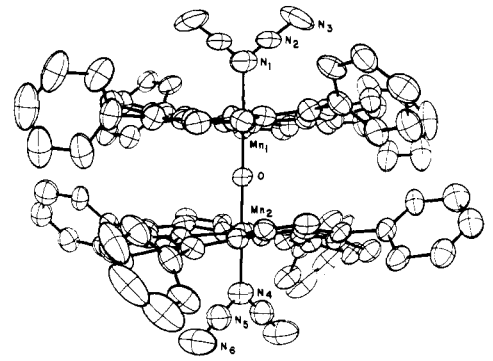

Figure 3. ORTEP[26] plot of $[N_3Mn^{IV}TPP]_2O$ viewed approximately perpendicular to the twofold axis. Atoms are represented by their vibrational ellipsoids plotted to represent the 50% probability surface. The terminal azide ligands are twofold disordered in the crystal.

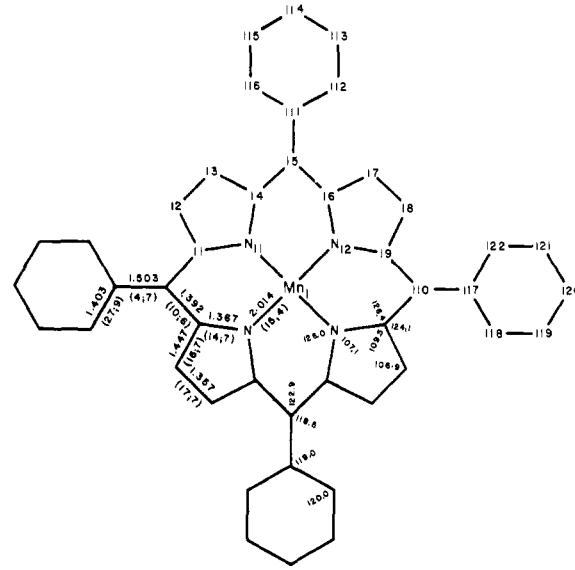

Figure 4. Formal diagram of the tetraphenylporphinato skeleton. The upper half of the diagram shows the numbering scheme for the unique atoms in the porphyrin ligated to Mn_1. The numbering of atoms in the porphyrin ligated to Mn_2 is obtained by changing the first digit of each number from "1" to "2". The average bond lengths and angles for chemically analogous bond types are entered on the lower half of the diagram. The first figure in parentheses below an averaged bond length is the mean deviation; the second is the esd for an individual determination; both are in units of 0.001 Å.

Other features of the infrared spectra related to the oxidation state of the complexes are as follows: (1) the absence of any intense bands in the 1270–1295 cm^{-1} region; (2) the antisymmetric stretching frequencies of the terminal axial ligands in both dimeric complexes are lower than the corresponding Mn(III) compounds (N_3MnTPP, 2033 cm^{-1}; $(N_3MnTPP)_2O$, 2010 cm^{-1}; (OCN)-MnTPP, 2165 cm^{-1}; $[(OCN)MnTPP]_2O$, 2160 cm^{-1}).

Magnetic Data. The magnetic susceptibility of **1**, determined both in the solid state and in solution, gave $\mu_{eff} = 2.0\ \mu_B$.

An ESR signal was not observed for the dimeric complexes, $[XMn^{IV}TPP]_2O$, at temperatures down to 8 K.

Description of Structure. Figure 3 is an ORTEP[26] drawing of the $(N_3MnTPP)_2O$ molecule viewed perpendicular to the crys-

(25) (a) Herzberg, G. "Molecular Spectra and Molecular Structure II. Infrared and Raman Spectra of Polyatomic Molecules"; Van Nostrand: New York, 1945; p 228. (b) Hastie, J. W.; Hauge, R. H.; Margrave, J. L. *High Temp. Sci.* **1969**, *1*, 76–85.

(26) Johnson, C. K. Report ORNL-3794; Oak Ridge National Laboratory: Oak Ridge, TN, 1965.

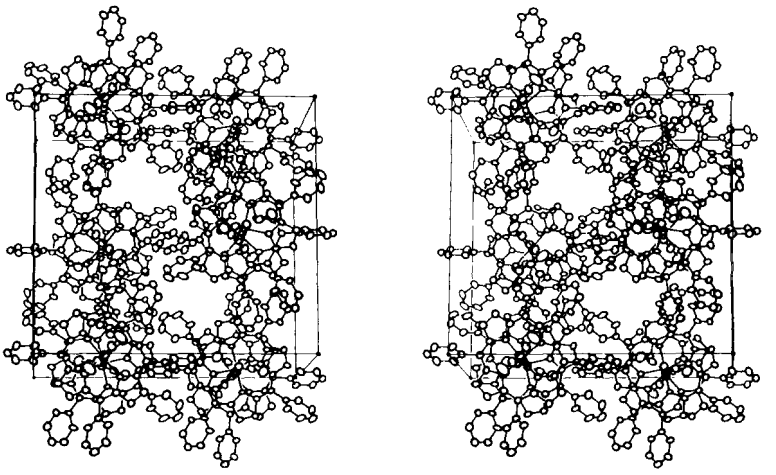

Figure 5. Stereoview of the crystal packing diagram for $[N_3Mn^{IV}TPP]_2O$. The two void channels are partially occupied by disordered chlorobenzene molecules.

Table III. Intramolecular Distances (Å)

porphyrin 1			porphyrin 2		
atom 1	atom 2	dist	atom 1	atom 2	dist
Mn1	O(oxo)	1.743 (4)	Mn2	O(oxo)	1.794 (4)
Mn1	N1	1.998 (8)	Mn2	N4	1.993 (7)
Mn1	N11	2.009 (4)	Mn2	N21	2.028 (4)
Mn1	N12	2.030 (4)	Mn2	N22	1.989 (3)
N11	C11	1.368 (6)	N21	C21	1.382 (6)
N11	C14	1.378 (6)	N21	C24	1.368 (6)
N12	C16	1.350 (6)	N22	C26	1.395 (6)
N12	C19	1.350 (6)	N22	C29	1.344 (6)
C11	C110	1.386 (7)	C21	C210	1.394 (6)
C11	C12	1.455 (7)	C21	C22	1.420 (6)
C12	C13	1.380 (7)	C22	C23	1.366 (7)
C13	C14	1.433 (7)	C23	C24	1.422 (6)
C14	C15	1.398 (6)	C24	C25	1.402 (6)
C15	C16	1.416 (6)	C25	C26	1.379 (6)
C16	C17	1.469 (7)	C26	C27	1.468 (6)
C17	C18	1.358 (7)	C27	C28	1.323 (6)
C18	C19	1.453 (7)	C28	C29	1.455 (6)
C19	C110	1.378 (7)	C29	C210	1.385 (6)
C15	C111	1.496 (7)	C25	C211	1.505 (6)
C110	C117	1.509 (7)	C210	C217	1.500 (6)
C111	C112	1.391 (7)	C211	C212	1.352 (7)
C112	C113	1.436 (7)	C212	C213	1.375 (7)
C113	C114	1.411 (8)	C213	C214	1.449 (8)
C114	C115	1.403 (8)	C214	C215	1.348 (8)
C115	C116	1.419 (7)	C215	C216	1.439 (7)
C116	C111	1.387 (7)	C216	C211	1.442 (7)
C117	C118	1.427 (9)	C217	C218	1.414 (8)
C118	C119	1.426 (9)	C218	C219	1.367 (8)
C119	C120	1.393 (11)	C219	C220	1.349 (11)
C120	C121	1.349 (11)	C220	C221	1.436 (11)
C121	C122	1.452 (8)	C221	C222	1.407 (9)
C122	C117	1.392 (8)	C222	C217	1.421 (8)
N1	N2	1.06 (1)	N4	N5	1.26 (1)
N2	N3	1.15 (1)	N5	N6	1.22 (1)
		Chlorobenzene			
Cl	Cl	1.67			
C	C	1.40			

[a] Fixed. Average.

tallographic C_2 axis. Each molecule possesses C_2 symmetry with both manganese atoms, the bridging oxygen atom, and the ligated nitrogen of each azide ligand lying on the crystallographic C_2 axis parallel to *b*. This requires the two porphyrinato cores of the dimer to be parallel and the Mn–O–Mn bond angle to be 180°. The molecule, excluding the axial azide ligands, exhibits approximate D_2 symmetry. The additional twofold axes relate C11 to C24 and C110 to C25, etc. (refer to Figure 4 for atom numbering).

The packing of the molecules in the unit cell forms channels in the crystal (Figure 5). Chlorobenzene partially occupies these channels.

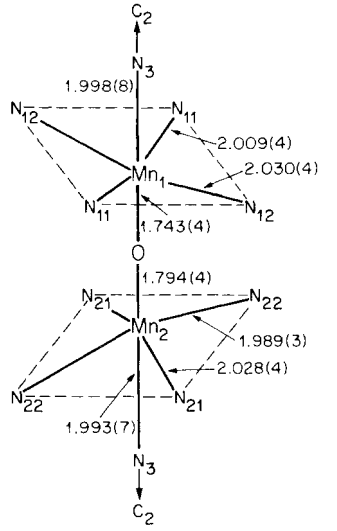

Figure 6. Coordination environment of the Mn–O–Mn moiety in $[N_3Mn^{IV}TPP]_2O$. (all distances in Å units).

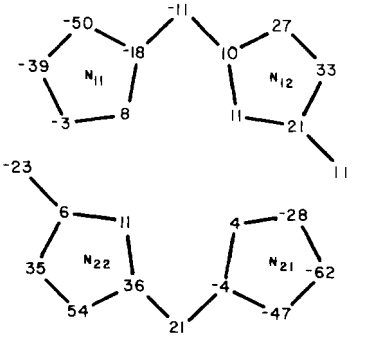

Figure 7. A formal diagram of the porphinato cores showing the displacement of each unique atom, in units of 0.01 Å, from the mean planes of the 24 atom cores. The upper half of the diagram shows the displacements for the porphyrin ligated to Mn1; the lower half is for the porphyrin ligated to Mn2. Twofold rotation of each about the center completes each porphyrin ring. A positive sign indicates a displacement moving the atom closer to the center of the molecule (i.e., closer to the bridging oxygen atom of the dimer).

The individual bond lengths and angles are listed in Tables III and IV. The atom numbering scheme for the porphyrinato ligands is shown in Figure 4. This figure also shows the averaged bond parameters for chemically analogous bond types.

The bond lengths within the manganese coordination sphere are shown in Figure 6. The manganese atoms are displaced from the mean N_4 planes of the two TPP ligands toward the bridging oxygen by 0.10 and 0.08 Å for Mn1 and Mn2, respectively. The

Table IV. Intramolecular Angles (Deg)

porphyrin 1				porphyrin 2			
atom 1	atom 2	atom 3	angle	atom 1	atom 2	atom 3	angle
O(oxo)	Mn1	N11	93.3 (1)	O(oxo)	Mn2	N21	93.3 (1)
O(oxo)	Mn1	N12	92.4 (1)	O(oxo)	Mn2	N22	91.3 (1)
N11	Mn1	N11[a]	173.5 (2)	N21	Mn2	N21[a]	173.3 (2)
N11	Mn1	N12	89.5 (2)	N21	Mn2	N22	90.1 (2)
N11	Mn1	N12[a]	90.2 (2)	N21	Mn2	N22[a]	89.7 (2)
N12	Mn1	N12[a]	175.3 (2)	N2^	Mn2	N22[a]	177.5 (2)
Mn1	N11	C11	125.3 (3)	Mn	N21	C21	125.6 (3)
Mn1	N11	C14	126.9 (4)	Mn2	N21	C24	126.0 (3)
C11	N11	C14	106.6 (4)	C21	N21	C24	107.0 (4)
Mn1	N12	C16	126.2 (3)	Mn2	N22	C26	125.2 (3)
Mn1	N12	C19	125.4 (3)	Mn2	N22	C29	127.1 (3)
C16	N12	C19	107.9 (4)	C26	N22	C29	107.1 (4)
N11	C11	C110	127.0 (4)	N21	C21	C210	124.5 (4)
N11	C11	C12	110.5 (4)	N21	C21	C22	108.9 (4)
C110	C11	C12	122.4 (4)	C210	C21	C22	126.6 (4)
C11	C12	C13	105.3 (5)	C21	C22	C23	108.2 (4)
C12	C13	C14	107.8 (5)	C22	C23	C24	106.1 (4)
C13	C14	N11	109.8 (5)	C23	C24	N21	109.6 (4)
C13	C14	C15	124.0 (5)	C23	C24	C25	124.3 (4)
N11	C14	C15	126.3 (5)	N21	C24	C25	126.0 (4)
C14	C15	C16	121.5 (4)	C24	C25	C26	122.7 (4)
C14	C15	C111	118.9 (4)	C24	C25	C211	117.1 (4)
C16	C15	C111	119.6 (4)	C26	C25	C211	120.2 (4)
C15	C16	N12	127.5 (5)	C25	C26	N22	126.5 (4)
C15	C16	C17	121.8 (4)	C25	C26	C27	125.5 (4)
N12	C16	C17	110.6 (5)	N22	C26	C27	107.7 (4)
C16	C17	C18	104.2 (4)	C26	C27	C28	107.6 (4)
C17	C18	C19	108.6 (5)	C27	C28	C29	107.5 (4)
C18	C19	N12	108.6 (4)	C28	C29	N22	110.0 (4)
C18	C19	C110	124.4 (5)	C28	C29	C210	123.6 (5)
N12	C19	C110	126.8 (4)	N22	C29	C210	126.4 (4)
C19	C110	C11	123.4 (5)	C29	C210	C21	123.9 (4)
C19	C110	C117	119.8 (4)	C29	C210	C217	118.5 (4)
C11	C110	C117	116.6 (4)	C21	C210	C217	117.6 (4)
C15	C111	C112	119.4 (5)	C25	C211	C212	121.6 (4)
C15	C111	C116	118.3 (4)	C25	C211	C216	117.2 (5)
C112	C111	C116	122.2 (5)	C212	C211	C216	121.1 (4)
C111	C112	C113	119.1 (5)	C211	C212	C213	120.9 (5)
C112	C113	C114	118.6 (5)	C212	C213	C214	119.9 (5)
C113	C114	C115	121.3 (5)	C213	C214	C215	119.9 (5)
C114	C115	C116	119.2 (6)	C214	C215	C216	120.6 (5)
C115	C116	C111	119.6 (5)	C215	C216	C211	117.4 (5)
C110	C117	C118	118.0 (6)	C210	C217	C218	118.9 (5)
C110	C117	C122	118.6 (6)	C210	C217	C222	119.9 (5)
C118	C117	C122	123.4 (6)	C218	C217	C222	121.2 (5)
C117	C118	C119	116.8 (7)	C217	C218	C219	119.9 (7)
C118	C119	C120	120.3 (8)	C218	C219	C220	120.9 (8)
C119	C120	C121	121.8 (7)	C219	C220	C221	121.2 (7)
C120	C121	C122	121.2 (8)	C220	C221	C222	119.8 (7)
C121	C122	C117	116.5 (7)	C221	C222	C217	117.0 (7)
Mn1	N1	N2	128.3 (7)	Mn2	N4	N5	125.0 (5)
N1	N2	N3	176.9 (14)	N4	N5	N6	178.2 (11)

[a] Fixed.

tetragonal distortion observed in six coordination manganese(III) porphyrin structures is absent.[27]

Both porphyrinato cores of the dimer are significantly nonplanar (Figure 7), displaying a quasi-S_4 type ruffling similar to that observed in $[Fe(TPP)]_2N$.[28] The dihedral angles between the mean planes of the 24-atom porphyrinato cores (P_c) and the individual pyrroles are N11 = −14.6°, N12 = 5.9°, N23 = −16.9°, and N22 = 11.5° (a positive sign is chosen to indicate a pyrrole tilted so as to move the β pyrrole carbon atoms closer to the center of the molecule). This distortion results in the separation of two mean P_c planes being 0.16 Å larger than the 3.72-Å separation of the two mean N_4 planes in the dimer.

The two porphyrins are twisted with respect to each other so as to lie approximately midway between a staggered and an eclipsed conformation, the N11–Mn1–Mn2–N21 torsion angle being −28.5°. This specific value for the twist angle is not forced by internal steric considerations, since all but one of the interplanar contacts are greater than 3.4 Å (C17–C28 = 3.35 Å). Intermolecular crystal packing forces are probably the determining factor.

Dihedral angles of −51.3°, 67.8°, 44.3°, and −56.2° are formed between the mean planes and the four unique phenyl groups linked to the porphyrins through atoms C111, C117, C211, and C217, respectively. The signs, but not the magnitudes, of these angles conform to the noncrystallographic D_2 symmetry of the molecule.

Discussion

The reaction of (tetraphenylporphinato)manganese(III) derivatives, $XMn^{III}TPP$, X = N_3^- and OCN^-, with iodosylbenzene produces dimeric μ-oxo-manganese(IV) porphyrin complexes **4**. A reasonable mechanism for the generation of these complexes is given in Scheme I.

Because nearly quantiative yields of **4** are obtained, the following

(27) Scheidt, W. R. In "The Porphyrins"; Dolphin, D., Ed.; Academic Press: New York, 1978; Vol. III, Chapter 10, p 474.

(28) Scheidt, W. R.; Summerville, D. A.; Cohen, I. A. *J. Am. Chem. Soc.* **1976**, *98*, 6623–6628.

Scheme I

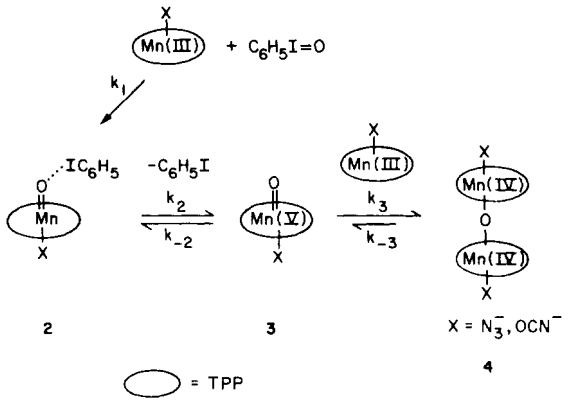

conclusion can be drawn on the basis of Scheme I: when X = N_3^- and OCN^-, $k_2 > k_1$, k_{-2} and $k_3 \gg k_2$. A mechanism for the incorporation of ^{18}O from water into the dimer complexes, which is consistent with Scheme I, invokes oxo–oxygen exchange in **3** prior to the capture of **3** by $XMn^{III}TPP$ to produce **4**. Such an oxo–oxygen exchange has been demonstrated for the reactive oxo(porphinato)chromium(V) complex of Groves and Kruper,[6] as well as for other transition-metal complexes.[29]

Properties of the Dimeric Complexes. The μ-oxo dimeric structure of compound **1** was determined by X-ray crystallography. Based on this structure, one can explain a number of spectral and magnetic properties. The broad IR absorption band at 794 cm^{-1} can be assigned to the Mn–O–Mn antisymmetric stretching fundamental, ν_3, based on ^{18}O labeling. The low magnetic moment and the absence of an EPR signal for **1** support an antiferromagnetically coupled dimeric structure. The dimeric nature of $[(OCN)MnTPP]_2O$ can then be inferred from its elemental analysis and its very high degree of spectral similarity to $(N_3MnTPP)_2O$.

That these compounds maintain the dimeric structure in solution is supported by several lines of evidence. (1) The infrared absorption band assigned to the Mn–O–Mn antisymmetric stretch is present in the dichloromethane solution spectra of these compounds. (2) If solvolysis of the dimer in solution to form monomeric Mn(IV) complexes were to occur, one would observe an EPR spectrum similar to the one observed for $Mn^{IV}TPP(OCH_3)_2$.[30] No such spectra are observed for solutions of the pure dimers. (3) Peaks due to $XMn^{III}(TPP)$ are absent from the electronic spectra of the pure dimers in solution, thus establishing that dissociation of **4** into **3** and XMn(TPP) (Scheme I) is slow at 23 °C. (4) The magnetic susceptibility of the dimers is the same in solution and solid state.

The lowest unoccupied molecular orbitals (LUMOs) of the 16-electron ligands N_3^- and OCN^- are the π_x^* and π_y^* antibonding orbitals. Electron donation into these orbitals would reduce the force constants, and hence the stretching frequencies, associated with these ligands. The lower stretching frequencies observed for X^- in the dimers vs. those found in the $XMn^{III}TPP$ complexes might be explained by greater electron donation into the LUMOs of X^- in the dimers due to the presence of the strongly donating oxo ligand trans to X^-. The XMnTPP complexes lack such a strongly coordinated trans ligand.[31] The lower stretching frequencies observed in the dimers could also be explained by greater donation of π-electron density from X^- to Mn(IV) vs. donation to Mn(III). However, since the highest occupied molecular orbitals (HOMOs) of the ligands, X^-, are nonbonding between the ligand atoms, the former explanation is favored.

In the preparation of high-valent metalloporphyrins there is the possibility of ligand-centered vs. metal-centered oxidation.[32] This leads to three possible ground electronic states for the MnTPP moieties in the dimeric complexes: (1) a high-spin (hs) manganese(III) antiferromagnetically coupled to a porphyrin cation radical, hs $Mn^{III}P^{+\cdot}$; (2) a low-spin (ls) manganese(III) antiferromagnetically coupled to a porphyrin cation radical, ls $Mn^{III}P^{+\cdot}$; (3) manganese(IV) in a neutral porphyrin, $Mn^{IV}P$. The crystallographic structural data are most consistent with the third formulation, $Mn^{IV}P$, for the ground electronic state of **1** at 23 °C, the temperature at which the diffraction data were collected.

Since the $d_{x^2-y^2}$ orbital is formally unoccupied in all six coordinate manganese(III) and manganese(IV) porphyrin complexes, one might expect to see a narrow range of equatorial bond lengths in these complexes. This is indeed found to be the case. The average Mn–N(porphyrin) bond lengths in the high-spin manganese(III) complexes $N_3MnTPP(CH_3OH)$[31] and ClMn(TPP)(pyridine)[33] are 2.031 and 2.009 Å, respectively. In the alternating high- and low-spin Manganese(III) porphyrin polymer of Scheidt and Reed, $[(Im)MnTPP]_n$,[34] the equatorial bond lengths are 2.020 (4) and 2.018 (5) Å. The average Mn–N bond length of 2.012 Å found in $Mn(TPP)(OCH_3)_2$[11] and the value of 2.014 Å found in **1** both lie within the range of values occurring in the Mn(III) structures.

Occupation of the d_{z^2} orbital in six-coordinate high-spin Manganese(III) porphyrin complexes leads to a tetragonal distortion with resultant long axial bonds.[27] For d^3 Mn(IV) complexes this effect should not be observed. A good model for estimating the difference in axial bond lengths between high-spin manganese(III) and manganese(IV) is the complex di-μ-oxotetrakis(2,2'-bipyridine)dimanganese(III,IV) perchlorate, which has been structurally characterized by Plaskin et al.[35] This binuclear mixed-valence complex has a high-spin Mn(III) atom and a Mn(IV) atom in nearly identical coordination environments. The difference in bond lengths to the axial nitrogen atoms in this complex is 0.194 Å. The 1.996 (7) Å Mn–N_3 bond length in **1** is 0.18 Å shorter than that found in the six-coordinate high-spin complex $N_3Mn^{III}TPP(CH_3OH)$,[31] in good agreement with the estimate of 0.19 Å found above. The effect of a change from high spin to low spin on the Mn(III)–axial ligand bond length is best estimated from the alternating high-spin, low-spin $[(Im)Mn^{III}TPP]_n$ polymer[34] to be about 0.11 Å.[36] On the basis of manganese–axial ligand bond length arguments, the best model from the MnTPP moieties of **1** is $Mn^{IV}TPP$.

Recently, Goff, Reed, and co-workers have reported the observation of an IR active porphyrin ring mode at ca. 1280 cm^{-1} in tetraphenylporphyrin cation radicals which provides a criterion for formulating the electronic structures of highly oxidized metalloporphyrin complexes.[37] These authors believe that this diagnostic criterion may have general applicability to the identification of porphyrin cation radicals.

The argument for metal-centered oxidation in the dimers is supported by the lack of any strong IR bands in the 1270–1295-cm^{-1} region of the spectra.

Acknowledgment. Support of this work by the National Science Foundation (Grant No. CHE 79-09730) and by the donors of the Petroleum Research Fund, administered by the American Chemical Society is acknowledged. The crystal structure analysis

(29) (a) Murmann, R. K. *J. Am. Chem. Soc.* **1974**, *96*, 7836–7837. (b) Sharpless, K. B.; Townsend, J. M.; Williams, D. R. *Ibid.* **1972**, *92*, 295–297.
(30) Camenzind, M.; Hill, C. L., unpublished work.
(31) Day, V. W.; Stults, B. R.; Tasset, E. L.; Day, R. O.; Marianelli, R. S. *J. Am. Chem. Soc.* **1974**, *96*, 2650–2652.
(32) (a) Fuhrhop, J. H. *Struct. Bonding (Berlin)* **1974**, *18*, 1–67. (b) Dolphin, D.; Niem, T.; Felton, R. H.; Fujita, I. *J. Am. Chem. Soc.* **1975**, *97*, 5288–5290. (c) Gans, P.; Marchon, J.; Reed, C. A. *Nouv. J. Chim.* **1981**, *5*, 203–204.
(33) Kirner, J. F.; Scheidt, W. R. *Inorg. Chem.* **1975**, *14*, 2081–2986.
(34) Landrum, J. T.; Hatano, K.; Scheidt, W. R.; Reed, C. A. *J. Am. Chem. Soc.* **1980**, *102*, 6729–6735.
(35) Plaksin, P. M.; Stoufer, R. C.; Mathew, M.; Palenik, G. J. *J. Am. Chem. Soc.* **1972**, *94*, 2121–2122.
(36) The $(ImMn^{III}TPP)_n$ polymer of Landrum et al.[34] actually contains alternating high-spin and low-spin manganese(III) atoms with the latter atoms in a spin equilibrium estimated to be 20–30% high spin and 70–80% low spin. If a correction is made for this high-spin component in the low-spin manganese(III) atoms, then the estimated change in Mn–axial ligand bond length for a change for high to low spin is 0.11 Å.
(37) Shimomura, E. T.; Phillippi, M. A.; Goff, H. M.; Scholz, W. F.; Reed, C. A. *J. Am. Chem. Soc.* **1981**, *103*, 6778–6780.

was performed at the U.C. Berkeley X-ray Crystallographic Facility (CHEXRAY). We are grateful to our co-worker Carol Balfe for her help in preparation of this manuscript.

Registry No. 1, 79775-62-5; **4** (X = OCN), 81602-67-7; $N_3Mn^{III}TPP$, 56413-47-9; iodosylbenzene, 536-80-1.

Supplementary Material Available: A listing of observed and calculated structure factors for the title compound (23 pages). Ordering information is given on any current masthead page.

Photochemistry of Alkyl Halides. 8. Formation of a Bridgehead Alkene[1]

Paul J. Kropp,* Paul R. Worsham, Robert I. Davidson, and Tappey H. Jones

Contribution from the Department of Chemistry, University of North Carolina, Chapel Hill, North Carolina 27514. *Received July 27, 1981*

Abstract: Irradiation of the bridgehead iodides **4**, **7**, and **10** afforded principally the ionic products **6**, **9**, and **12** accompanied by small amounts of the reduction products **5**, **8**, and **11**. Studies in methanol-*d* indicated an absence of pathways leading to ethers **6**, **9**, and **12** involving bridgehead alkene or propellane intermediates. By contrast, the iodo ether **16** afforded not only the epimeric endo iodide **17**, the reduction product **19**, and the expected ionic products **23**, **24**, **27**, and **28** but also the rearranged iodide **25** and the ketals **26**. Deuterium labeling and trapping studies showed that these latter products arise via the intermediacy of the bridgehead alkene **20**. By contrast, the iodo lactone analogue **48** afforded only the reduction product **50** and the ionic products **51**, **52**, **54**, and **55**, with no detectable formation of products attributable to the intermediacy of the bridgehead alkene **61**. The factors involved in the formation of bridgehead alkene intermediate **20** are discussed.

Previous studies in these laboratories have shown that irradiation of alkyl iodides in solution is a powerful and convenient method for the generation of carbocations, via a process thought to involve initial light-induced homolytic cleavage of the carbon–iodine bond followed by electron transfer within the initially formed caged radical pair (Scheme I).[2] The powerfulness of the method was demonstrated by formation of the difficultly accessible 1-bicyclo[2.2.1]heptyl cation; irradiation of 1-iodobicyclo[2.2.1]heptane (**1**) in methanol or diethyl ether afforded principally the ether **3** (Y = OCH_3 or OC_2H_5), accompanied by a small amount of the radical product bicyclo[2.2.1]heptane (**2**).[2a]

Similar studies involving other alkyl systems have revealed a marked propensity for carbocations generated photolytically from

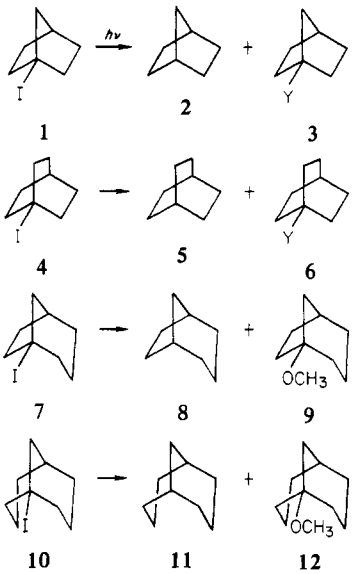

iodides to undergo 1,2 or 1,3 deprotonation in competition with nucleophilic trapping, even in alcoholic media.[2a,3] However, similar deprotonation of the 1-bicyclo[2.2.1]heptyl cation would afford either the bridgehead alkene **13** or the propellane **14**, each

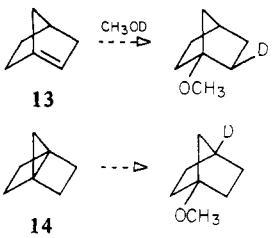

(1) (a) Part 7: Kropp, P. J.; Pienta, N. J.; Sawyer, J. A.; Polniaszek, R. P. *Tetrahedron* **1981**, *37*, 3229–3236. (b) For a preliminary report of a portion of this work, see: Kropp, P. J.; Jones, T. H.; Poindexter, G. S. *J. Am. Chem. Soc.* **1973**, *95*, 5420–5421.

(2) (a) Kropp, P. J.; Poindexter, G. S.; Pienta, N. J.; Hamilton, D. C. *J. Am. Chem. Soc.* **1976**, *98*, 8135–8144. (b) A number of reports have appeared concerning the photosolvolysis of aralkyl halides: Zimmerman, H. E.; Sandel, V. R. *Ibid.* **1962**, *85*, 915–922. Ivanov, V. B.; Ivanov, V. L.; Kuz'min, M. G. *J. Org. Chem. USSR (Engl. Transl.)* **1973**, *9*, 345–347. Cristol, S. J.; Greenwald, B. E. *Tetrahedron Lett.* **1976**, 2105–2108. Appleton, D. C.; Brocklehurst, B.; McKenna, J.; McKenna, J. M.; Thackeray, S.; Walley, A. R. *J. Chem. Soc., Perkin Trans. 2* **1980**, 87–90. Slocum, G. H.; Kaufmann, K.; Schuster, G. B. *J. Am. Chem. Soc.* **1981**, *103*, 4625–4627. The last authors have recently presented evidence supporting the following mechanism for the photomethanolysis of 1-(iodomethyl)naphthalene:

$$RI \xrightarrow{h\nu} R\cdot + I\cdot$$

$$RI + I\cdot \rightarrow RI_2\cdot$$

$$RI_2\cdot + CH_3OH \rightarrow ROCH_3 + H^+ + I_2^-$$

Although such a mechanism may ultimately be found to be general for aralkyl iodides, it apparently does not apply, at least generally, to alkyl systems. Thus, the quantum yield for the formation of ether **3** (Y = OCH_3) from iodide **1** is substantially decreased by the presence of oxygen,[2a] in agreement with the mechanism of Scheme I but not that outlined above. Moreover, preliminary studies in these laboratories have shown that the quantum yield for photoconversion of 1-iodooctane is independent of the concentration of iodide **1**. Finally, iodide **1** is inert in a methanolic solution containing I·, generated by irradiation of iodine at >280 nm.

(3) Kropp, P. J.; Gibson, J. R.; Snyder, J. J.; Poindexter, G. S. *Tetrahedron Lett.* **1978**, 207–210.

0002-7863/82/1504-3972$01.25/0